Lasers in Manufacturing Conference 2025

Laser metal powder bed fusion of pure copper with green and infrared wavelength for power electronics applications

Isabelle Günther[a,b,1], Benjamin Zillmann[a], Thomas Niendorf[b]

[a]*Robert Bosch GmbH, Robert-Bosch-Campus 1, 71272 Renningen, Germany*
[b]*Institute of Materials Engineering, University of Kassel, Mönchebergstr. 3, 34125 Kassel, Germany*

Abstract

Power electronics feature small functional structures, which are preferably made of pure copper and are built on sensitive ceramic-based substrates, so called Direct Bonded Copper (DBC) substrates. A novel additive manufacturing (AM) approach employs the laser powder bed fusion (PBF-LB/M) process to manufacture the functional structures directly onto the DBC, eventually enabling the reduction of manufacturing cost and effort. Processing of pure copper in the PBF-LB/M process is challenging due to its reflectivity and its thermal conductivity. Additionally, using a DBC in the PBF-LB/M process leads to complex multi-material interactions. Focusing on the application, the processability of pure copper with a green and an infrared laser in the same machine setup was investigated. The influence of laser wavelength and process parameters on the resulting part properties was analyzed, differences between both wavelengths were pinpointed, and suitable parameter sets were identified.

Keywords: additive manufacturing; laser powder bed fusion; ceramic-based substrate; pure copper; laser wavelength

1. Introduction

Power modules, known as packaging of power electronics, typically utilize so called Direct Bonded Copper (DBC) substrates, which are based on a ceramic core with a copper metallization on both sides. The ceramic core enables electrical insulation between both sides of the DBC substrate while the copper metallization offers high thermal and electrical conductivity. Small metallic functional structures, known as spacers, are used for the semiconductor attachment on top of the DBC substrate (Lin und Liu 2020). Separate assembly processes, for example silver sintering, including pick-and-place, are required to attach the functional structures to the semiconductors and the DBC substrate. Therefore, a precise dimensional accuracy and a high surface quality of the structures is important. The defined surface roughness of the functional structures is similar to the surface quality of the DBC substrates (Ra ≤ 3 µm) (Rogers Corporation 2025). Additionally, the functional structures facilitate thermal and electrical connections between substrate and semiconductor or between the different substrates (Lin und Liu 2020). This requires functional structures, which have high thermal and electrical conductivity and are closely bonded to the substrate or semiconductor, thus minimizing the thermal resistance, and maximizing the heat dissipation within the power module. Current manufacturing methods, such as precision punching, limit the lateral dimensions of the structures and result in high costs due to the small feature sizes. To address these challenges, a novel additive manufacturing (AM) approach is presented that leverages the laser powder bed fusion (PBF-LB/M) process to manufacture the functional structures directly onto the DBC substrate. The manufacturing takes place in one single manufacturing step, thereby reducing manufacturing costs and complexity. While pure copper is advantageous for power electronics due to its excellent physical and mechanical properties, it presents significant challenges for laser-based processing in the PBF-LB/M process. Pure copper exhibits a low absorptivity for laser radiation, resulting in only a small share of the applied energy being available to melt the powder material (Horn et al. 2022). For laser radiation with a

* Isabelle Günther. Tel.: +49(711)811-45630
E-mail address: Isabelle.guenther@de.bosch.com

wavelength of 1060 nm ≈ λ ≈ 1080 nm (referred to as infrared laser in the following text), which is commonly used in state-of-the-art PBF-LB/M machines, the absorptivity of pure bulk copper material is only between 3 % and 5 % (Punzel et al. 2020). The absorptivity of copper for laser radiation is also temperature-dependent (Punzel et al. 2020). During the PBF-LB/M process, copper undergoes a phase transition from solid to liquid. Upon reaching the melting temperature, the absorptivity of copper increases abruptly (Punzel et al. 2020). Additionally, due to the high thermal conductivity of pure copper the deposited thermal energy is rapidly conducted from the melt pool and dissipated into the surrounding area (Campagnoli et al. 2021). These challenges can lead to unstable process conditions when processing pure copper with infrared lasers, making it difficult to develop suitable process parameters (Campagnoli et al. 2021).

To mitigate the challenges of laser-based processing of copper and to maintain high conductivity, several strategies have been proposed for PBF-LB/M processing of pure copper. Firstly, the use of laser sources with shorter wavelengths can increase the absorptivity of copper. For laser radiation with a wavelength of λ ≈ 515 nm (referred to as green laser in the following text), the absorptivity of pure bulk copper material increases to around 40 % (Punzel et al. 2020). However, such lasers are currently only used in dedicated PBF-LB/M machinery. The low beam quality of commercially available green lasers leads to focal diameters of around 200 µm [9], which leads to relatively low power densities. The principal feasibility of using green lasers for the PBF-LB/M process has already been proven in literature (Horn et al. 2022; Hecht et al. 2024; Gruber et al. 2021). Densities close to 100 % were achieved, when pure copper was processed on a massive stainless steel build plate in the form of cubic samples (10 x 10 x 15 mm^3) and vertical walls (20 x 20 mm^2 and up to 3 mm thick) (Gruber et al. 2021). For their investigations they used a green TruDisk1020 disk laser (Trumpf SE + Co KG, Ditzingen, Germany) with a focus diameter of 200 µm and a maximum power of 500 W (Gruber et al. 2021). However, the authors emphasized that a fine structure (< 0.5 mm) is difficult to be realized as solidified droplets form on the as-built part surface (Gruber et al. 2021). Similar results were reported by Horn et al., Domine et al. and Hecht et al. with the same green TruDisk 1020 laser with focal diameters of 200 µm to 220 µm for single tracks and thin walls or specific copper structures (5 x 5 x 5 mm^3) (Horn et al. 2022; Domine et al. 2023; Hecht et al. 2024). Nordet et al. successfully minimized the focal diameter of the green laser to 90 µm by shortening the focal length during manufacturing of 15-mm cubic samples. This enhances the surface quality of the manufactured parts (Nordet et al. 2024). Nevertheless, a short focal length significantly limits the deflection of the laser beam and reduces the number of parts that can be manufactured per build job. As a result, this limitation poses a challenge in mass production scenarios, such as in power electronics, where millions of parts are produced annually.

Infrared lasers with high laser power are used to increase the energy input when processing copper. Infrared lasers are characterized by a high beam quality, which enables focusing of the laser beam eventually promoting high laser power densities in the PBF-LB/M process. Experimental studies show that a laser power above 400 W is necessary to produce dense pure copper parts (Lykov et al. 2016), however, commercial high-power lasers have only been available for the PBF-LB/M process for a few years. In the study of Jadhav et al. it was possible to manufacture cubic samples (10 x 10 x 7 mm^3) onto a pure copper baseplate with densities above 96.3 % by using an infrared laser with a laser power of 500 W and a small focal diameter of 37.5 µm (Jadhav et al. 2019). Ikeshoji et al. built cube specimens with dimensions of 10 x 10 x 10 mm^3 onto a pure copper baseplate with an infrared laser with a laser power of 800 W, resulting in a part density of around 96% (Ikeshoji et al. 2018). Similar results were achieved by Colopi et al. with an infrared laser with a laser power between 800 W and 1000 W for manufacturing cubic samples (5 x 5 x 5 mm^3) on a 316L base plate (Colopi et al. 2019). However, Jadhav et al. demonstrated that back reflections could damage the optical components of the PBF-LB/M machinery, and physical properties of copper still lead to narrow process windows and melt pool instabilities (Jadhav et al. 2019). Most findings regarding the processing of pure copper, whether using green or infrared lasers, focus on single tracks, walls, or parts of relatively large sizes. There is a lack of systematic research investigating the processability of pure copper for functional structures with small dimensions, typical used in power electronics applications. Studies addressing the manufacturing of functional structures on ceramic-based substrates with a thin metallization, such as DBC substrates, are not available, yet.

In most components manufactured by PBF-LB/M processes, the interactions between the AM structure and the base plate have been subject to limited research. Conventionally, the desired AM structure is separated from the base plate in a post-processing step. Also, for repair applications, where small features are additively added onto a conventionally manufactured base body, the base body typically consists of massive, large, metallic components and is made from conventional materials like tool steels and nickel alloys (Megahed et al. 2022; Wang et al. 2024). This makes it almost impossible to apply the findings to the intended application in the present publication. For power electronics, the functional structures are usually manufactured directly on the DBC substrate and both, the substrate and the manufactured AM structure, are integral parts of the final product. It is well known that the type (material and geometry) of the base plate and its thermal conductivity significantly influence the powder bed temperature and the process stability (Stoll et al. 2019; Colopi et al. 2019). When using ceramic-based DBC substrates with copper metallization in the PBF-LB/M process, the heat dissipation through the substrate changes significantly compared to conventional bulk metal plates, as the copper metallization and the ceramic core feature fundamentally different properties. Additionally, there is a significant risk of

substrate damage during the PBF-LB/M process, due to the limited thermal shock resistance and high sensitivity to tensile residual stresses of ceramic materials (Stoll et al. 2019). Cracks in the ceramic layer, no matter what type or size of cracks, deteriorate electrical insulation and reduce the heat dissipation from the chip to the cooling system (Gaiser et al. 2020).

The literature review clearly shows that processing of pure copper in the PBF-LB/M process is an emerging topic and both approaches, i.e., short-wavelength green lasers and high-power infrared lasers, have advantages and disadvantages. However, a direct comparison of lasers of both wavelengths is difficult, as the lasers are mostly integrated into different PBF-LB/M machinery, leading to changes in boundary and processing conditions. Additionally, most of the results for processing pure copper in the PBF-LB/M process are based on single tracks, walls, or parts with relatively large dimensions. No systematic studies have been carried out on the feasibility of processing pure copper for small functional structures, especially not on a thinly metallized ceramic-based substrate, i.e., DBC substrates. Therefore, the objective of the present publication is the systematic analysis of the processability of pure copper, focusing on the influence of the laser wavelength, a green and an infrared laser, on the part properties, such as the optical appearance and the density of the structures, the grain structure and its orientation as well as the thermal conductivity of the structures. Both lasers are integrated in the same PBF-LB/M machinery and therefore utilized under the same boundary conditions. In this context, the manufacturing of small functional structures on the thin copper metallization of the ceramic-based DBC substrate is assessed. Focusing on the envisaged mass production, the AM structures are examined and characterized in their as-built state. The effects of the PBF-LB/M process on the DBC substrate, such as the formation of cracks in the DBC ceramic, will be analyzed in future.

2. Material and methods

2.1. Ceramic-based DBC substrate and Cu powder material

The ceramic-based substrate used in the present study is a DBC substrate, as shown in Appendix A1a, supplied by Rogers Corporation (Chandler, Arizona, United States) with the dimensions given in Appendix A1b and A1c. The manufacturing process of the DBC substrate is described in (Hromadka et al. 2014). Due to its brittle material behavior and its limited thermal shock resistance, the ceramic is susceptible to tensile residual stress and steep temperature gradients (Gaiser et al. 2020). The metallization of the DBC substrate consists of pure copper, which exhibits high thermal and electrical conductivity (Gaiser et al. 2020). Notably, the thermal expansion coefficients of the copper metallization and the aluminum oxide ceramic differ, potentially resulting in residual stress states upon manufacturing in the DBC substrate (Gaiser et al. 2020). In the present investigations, pure copper powder sourced from Sandvik Osprey Ltd. (Neath, Wales, United Kingdom) was used. The chemical composition of the copper powder is as follows: > 99.85 wt% Cu (copper), < 0.1 wt% O (oxygen) and < 0.05 wt% Fe (iron). Due to an atomization under nitrogen, the powder particles exhibit a spherical morphology with a smooth surface, and the particle size distribution ranges from 15 µm to 45 µm.

2.2. PBF-LB/M system and design of experiments for process optimization

Relevant details on the specific PBF-LB/M system are reported in the following. Any further details are intellectual property (IP) of Robert Bosch GmbH. For the PBF-LB/M processing an in-house developed open system, with an argon gas atmosphere and a powder coater with brushes, was utilized. The direction of the gas flow and the direction of the coater in relation to the base plate are shown in Figure 2a. The system includes two lasers with different wavelength, one green and one infrared laser. A comparison of the two lasers is detailed in Appendix A2. Due to the machine configuration, the beam diameter of the green laser is about 130 µm larger compared to the same laser source reported for different machine configurations in several literature studies (Hecht et al. 2024; Gruber et al. 2021; Horn et al. 2022). Because of the large beam diameter, the available laser power to be distributed over a large area is characterized by relatively low power density. The high focal length, along with the low beam quality of the green laser, results in the increased focal diameter mentioned. When processing with the infrared laser, the power density is very high. Figure 1 shows the qualitative intensity distributions of the beam profiles (see Figure 1a: green laser and Figure 1b: infrared laser) in the focal plane. The intensity distribution of the green laser approximates a flattened Gaussian intensity distribution, whereas the intensity distribution of the infrared laser follows a sharp Gaussian profile with an intensity in the outer areas of the laser beam close to Zero. Characteristics

were analyzed with a beam profile camera Newport LBP2-HR-VIS2 (Newport Corporation, Irvine, California, United States of America).

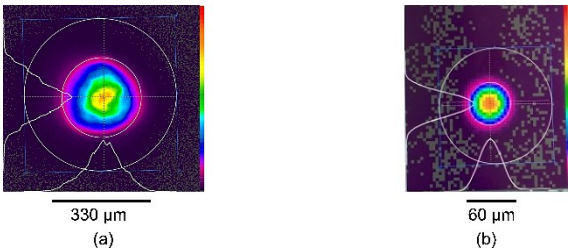

Figure 1: Beam profiles of the used lasers in the focal plane: a) green laser with a large focal diameter and a flattened Gaussian intensity distribution and b) infrared laser with a small focal diameter and a sharp Gaussian intensity distribution.

For process parameter development, a total of 16 cuboid structures were arranged equidistantly on top of the DBC substrate, as depicted in Figure 2a. The dimensions of these structures, each 3 × 3 x 1.8 mm³, were designed in light of literature values, i.e., die areas of silicon carbide (SiC) mosfets (Shi et al. 2023). The horizontal and vertical distances from the edge of each structure to the edge of the DBC substrate were set to 4.5 mm. Additionally, the spacing between adjacent samples on the DBC substrate was set to 6.6 mm in the x-direction and 7 mm in the y-direction. The samples were manufactured sequentially, progressing from sample 1 to sample 16 within a single layer. A layout with a single sample in the center on top of the DBC substrate, shown in Figure 2b, was used to analyze the sample properties without any influence of adjacent samples. For both lasers, the process parameter sets that lead to the highest sample density within the process parameter window considered, were used to manufacture the single sample layout.

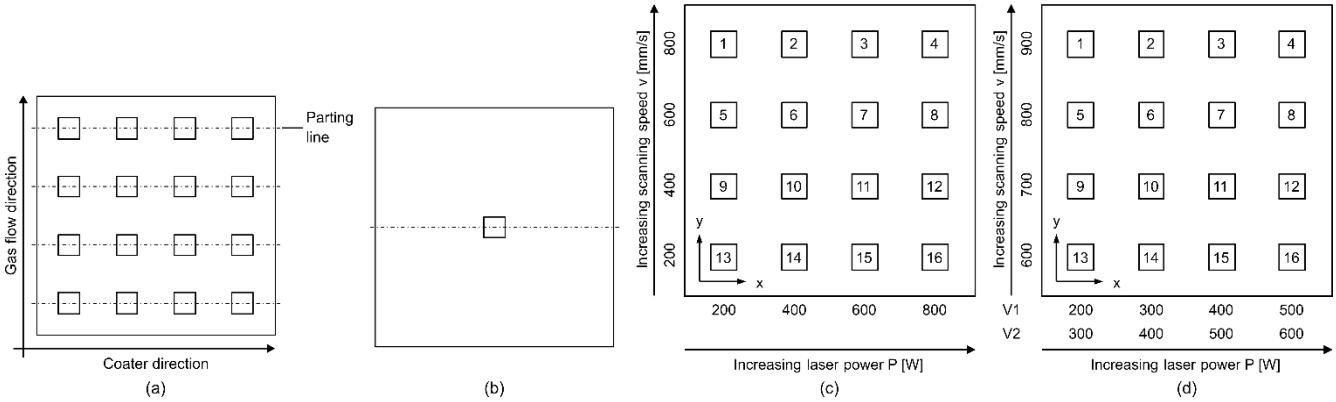

Figure 2: Build layout for 3 x 3 mm² copper structures on DBC substrate: layout for (a) process parameter development and (b) analysis of single sample as well as indication of laser power *P* and scanning speed *v* for samples manufactured with (c) green laser and (d) infrared laser.

As laser power P and scanning speed v have a significant influence on the volume energy density, they were systematically varied within the process parameter study. Their allocation to the samples is highlighted in Figure 2c for the green and in Figure 2d for the infrared laser. The hatch distance h, the layer thickness s as well as the hatch pattern, a linear bidirectional scan strategy with a rotation of 90° per layer and without contour, were maintained as constant parameters. The volume energy densities Ev, quantifying the energy delivered from the laser to the powder bed per unit volume, were calculated using Equation (1), a measure well-established in literature (Prashanth et al. 2017). This calculation method is primarily utilized to compare various studies concerning process parameters and energy input. Alternative approaches, such as calculating volume energy density based on focal diameter (Horn et al. 2022) or determining the normalized enthalpy (Ghasemi-Tabasi et al. 2020), are also mentioned in the literature. However, these methods have not yet gained widespread acceptance.

$$Ev = \frac{P}{v\ x\ h\ x\ s} \tag{1}$$

The detailed process parameters, both varied and constant, are summarized in Appendix A3. All samples were analyzed in their as-built condition. The hatch distance was determined in preliminary tests for pure copper powder with regard on the sample density (in the core volume). For reasons of brevity, these preliminary tests are not presented here.

2.3. Procedure and equipment used in the experimental investigations

The overview image of the DBC substrate (Appendix 1a) was captured using a Keyence VR 5000 profilometer (Keyence Deutschland GmbH, Neu-Isenburg, Germany). Following the fabrication of the structures via the PBF-LB/M process, the initial focus was directed towards evaluating the overall appearance and the density of the samples. The densities of the samples were analyzed in the cross section. The samples were cut line by line (refer to Figures 2a and 2b, Chapter 2.2). Each evaluated cross section was located at the center of the sample and oriented parallel to the build direction, perpendicular to the scan vectors in the top layer. The DBC substrate was sectioned with a diamond cut-off wheel and embedded in epoxy resin for cross sectional analysis. The embedding process was conducted under vacuum at ambient temperature. Metallographic grinding was performed stepwise using diamond grinding discs with grit sizes of 80, 220, 500, and 1200, followed by stepwise polishing with diamond suspensions of 6 µm, 3 µm, and 1 µm. The Keyence VR 5000 profilometer was employed for the overview images of the AM samples on top of the DBC substrate (Figure 3). A Keyence VHX 7000 microscope (Keyence Deutschland GmbH, Neu-Isenburg, Germany) was utilized for capturing the images of the top surface of the samples (Figures 5a and 5b). For the cross-sectional images of the samples (Figures 5c and 5d), a Zeiss Axio Imager.M1m (Carl Zeiss Microscopy Deutschland GmbH, Oberkochen, Germany) was used. The sample density was determined optically using Olympus Stream Essentials software, Version 2.3.3 (Evident, Tokyo, Japan), employing the threshold method. Only the core of the samples was considered for density determination to avoid miscalculations due to edge effects. For microstructure analysis, the samples were etched using a ferric nitrate solution.

Electron backscatter diffraction (EBSD) measurements were performed for analyzing the orientation of grains of the AM samples. The texture was investigated using the cross section of a sample, manufactured in the single sample layout. The cross sections were prepared with the standard procedure and additionally ion polished before EBSD measurement. A scanning electron microscope Quattro-S 21.0.0 (Thermo Fisher Scientific Inc., Waltham, Massachusetts, United States of America) was used for EBSD measurements. The measurements were performed with AZtec software, Version 6.2, and analyzed with AZtecCrystal software, Version 3.3, (both: Oxford Instruments, Abingdon, United Kingdom).

The thermal conductivity of the AM samples was determined by thermal interface material (TIM) testing. For the analysis of the thermal conductivity, three samples were manufactured for both the green and the infrared laser, with the dimensions 3 x 3 x 5 mm³ on top of a DBC substrate. The sample height was increased to achieve a sufficient gauge length for TIM testing. The parameter sets were selected, which achieved the highest sample density in process parameter development. The AM samples were separated from the DBC substrate by electrical discharge machining (EDM) and the density of the samples was verified using computer tomography (CT). A conventionally manufactured bulk copper sample was chosen as reference sample. The resulting temperature difference in the sample was recorded using a VarioCAM® HD head 980 camera (InfraTec GmbH, Dresden, Germany) with an additional close-up lens (temperature resolution: 0.02 K) and the samples were coated with graphite to generate a defined emissivity. Using Formula (2), the thermal conductivity of the sample $\lambda_{th,\,Sample}$ was determined as a function of the cross section of the sample A_{Sample}. The analyzed cross-sectional area of the sample therefore has a direct effect on the thermal conductivity values. $\dot{Q}$ is the heat flow that is applied to the sample during the measurement. Here, dT_{Sample}/dz_{Sample} resembles the temperature gradient that forms within the sample as a function of the measurement location over the sample height.

$$\lambda_{th,\,Sample} = \frac{\dot{Q}}{A_{Sample} * \frac{dT_{Sample}}{dz_{Sample}}} \qquad (2)$$

3. Results and discussion

3.1. Analysis results of the samples

In Figure 3, the structures of both lasers, the green (see Figure 3a) and the infrared laser (see Figure 3b), are displayed. By utilizing the green laser, it was not possible to manufacture fully bonded samples on the DBC substrate below laser powers of 400 W, independent of the used scanning speed. Here, only powder particles stick on top of the DBC metallization, or the samples show delamination at their edges. By increasing the laser power of the green laser to 600 W or 800 W, regardless of the investigated scanning speeds, fully bonded samples can be built up on top of the DBC substrate.

In case of all samples manufactured with the green laser, a rim of sintered but not completely melted powder particles is visible on the side surfaces of the samples. These particles cause a high surface roughness as well as wide radii at the corners and the side surfaces of the samples. When using the infrared laser, fully bonded samples can be manufactured on top of

the DBC substrate with a laser power of above 300 W, regardless of the applied scanning speed. At a laser power above 500 W, the infrared laser ablates the copper metallization of the DBC substrate and destroys the ceramic, regardless of the scanning speed used. The corresponding build job therefore had to be stopped and is not shown here. The contours (corners and edges) of the structures manufactured with the infrared laser are sharply defined for all parameter combinations and therefore significantly improved compared to the results of the green laser. However, for both lasers, the surface roughness of the AM samples does not meet the surface requirements typically associated with the conventional manufacturing approach (i. e. surface roughness of DBC substrates: Ra ≤ 3 µm). This is already visually apparent; therefore, no further measurement of the surface quality was performed.

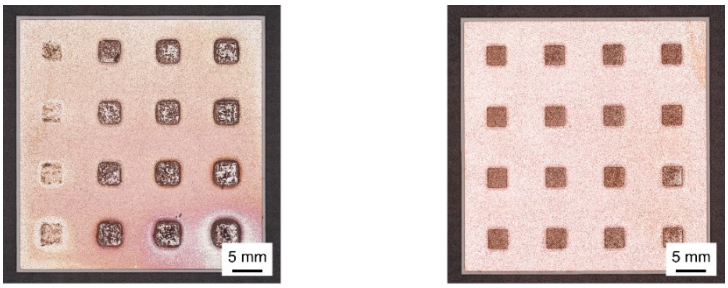

Figure 3: AM samples of both lasers on the DBC substrate: (a) samples manufactured with green laser and (b) samples manufactured with infrared laser.

As shown in Figure 4, for both lasers, the green (see Figure 4a) and the infrared (see Figure 4b), it was possible to determine a systematic correlation between the process parameters and the density (within the core) of the samples. With increasing laser power and decreasing scanning speed, resulting in an increasing energy input, the density of the samples increases. An interpolation was applied to directly compare the different densities resulting from different process parameters. Nevertheless, the present assessment primarily aims to identify trends related to how the different wavelengths and process parameters affect the properties of the parts produced. Additional research is needed to explore the interpolated regions. For both wavelengths, it was possible to manufacture samples with very high density close to 100 % on top of the DBC substrate, however, the process window is very narrow, and a high energy input is necessary. For the green laser, a maximum sample density of 99.9 % at a laser power of 800 W, a scanning speed of 200 mm/s and a resulting volume energy density of 1333.34 J/mm³ could be achieved. For the infrared laser, a laser power of 500 W, a scanning speed of 600 mm/s and a volume energy density of 347.22 J/mm³ are necessary to manufacture samples with a maximum density of 99.9 %. The volume energy density required to achieve the maximum sample density for the green laser (Ev = 1333.34 J/mm³) is about four times higher than the volume energy density in case of the infrared laser (Ev = 347.22 J/mm³). The focal diameter and the intensity distribution of the two lasers differ significantly. Eventually, this leads to energy density values in completely different ranges. In addition, also when considering only one laser, different process parameter combinations can lead to the same volume energy density. Sample 7 (P = 400 W, v = 800 mm/s) and sample 14 (P = 300 W, v = 600 mm/s) of the infrared laser were both manufactured with a volume energy density of 208.33 J/mm³, but the sample densities of both samples differ from each other. The volume energy density therefore has only limited significance when comparing pure copper components processed at different wavelengths.

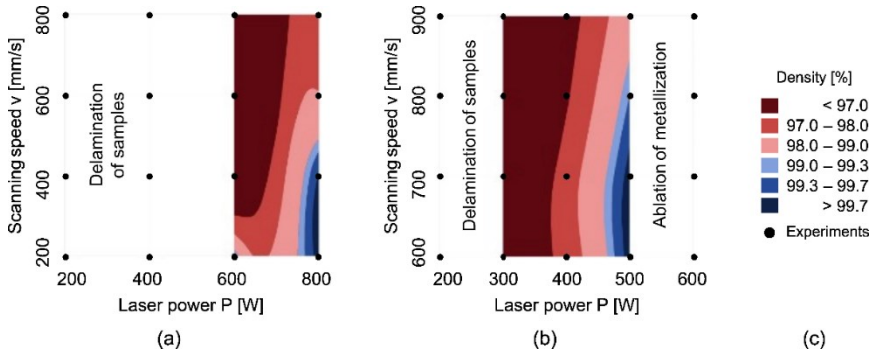

Figure 4: Influence of the process parameters on the density of the samples for both lasers: (a) samples manufactured with green laser, (b) samples manufactured with infrared laser and (c) legend of contour diagrams.

With the parameters leading to the highest densities of the samples in the build jobs for process development, single samples (see layout in Figure 2b) were manufactured on top of a DBC substrate. Pictures of the top surface and the cross section of the samples for both lasers are shown in Figure 5. Figure 5a shows the top surface and Figures 5c shows the cross section of the green laser sample. The top surface has a metallic appearance, and at the top surface of the sample continuous scan vectors are visible. This indicates that the copper is completely melted. The top surface exhibits a significant level of unevenness, so that the surface quality of the sample was not further investigated. As already described in the process development, a rim of sintered particles appears on the side surfaces of the sample. The sample has a very high density of 99.9 % (in the bulk volume) and the sample is completely bonded to the DBC metallization. No cracks are visible in the ceramic of the DBC substrate. In Figure 5b the top surface and in Figure 5d the cross section of the infrared laser sample are illustrated. In contrast to the green laser, the surface of the sample is flat and has no significant melting defects. The top surface is fully melted, and continuous scan vectors are visible. No sintered particles are visible on the side surfaces of the sample, leading to a defined contour of the sample geometry. As with the green laser, the sample has a very high density of 99.9 % and the ceramic of the DBC substrate is crack-free. Thus, the results of both layouts are transferable and there appears to be no or only slight interaction between adjacent samples.

The high density of the samples from both lasers allows a direct comparison of their microstructure. For the samples of both lasers, the grains grow alongside build direction, extending in a columnar shape throughout the entire height of each sample. Towards the top surface and the edges of the samples, the grains become finer and align slightly in the hatching direction. The microstructure of the green laser sample (see Figure 5c) is characterized by an irregular formed and very coarse grain structure. The microstructure of the infrared laser sample (see Figure 5d) is also irregular formed, but generally finer than the microstructure of sample manufactured with the green laser. The microstructure is strongly dominated by the hatching in the PBF-LB/M process (which is not visible for the green laser). It is not possible to reliably determine the exact grain size for any sample due to the highly irregular shape of the grains.

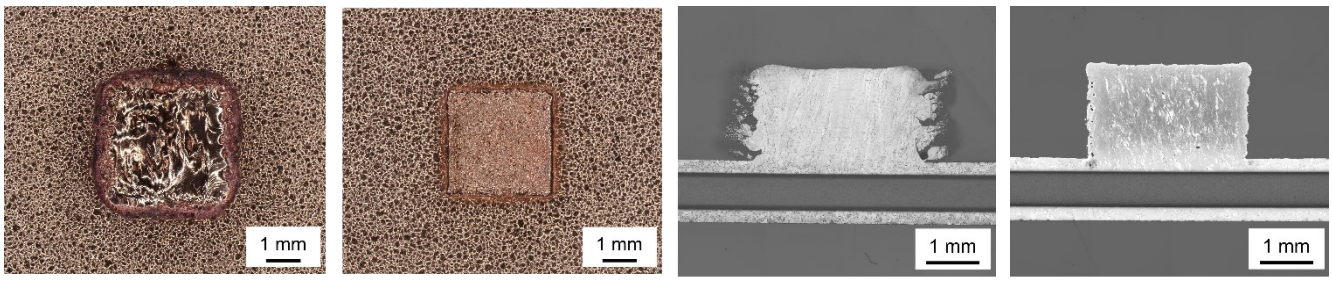

Figure 5: Samples manufactured with high-density process parameter sets for both lasers: top surface of sample manufactured with (a) green laser and (b) infrared laser as well as microstructure analysis of sample manufactured with (c) green laser and (d) infrared laser.

For both lasers, epitaxial grain growth is predominant, originating from the grains of the DBC metallization. The grain structure of the metallization acts as the nucleus for the development of the grain structure in the AM sample. For the green laser sample, however, the grain structure of the metallization is only slightly influenced by the PBF-LB/M process on the surface of the DBC substrate compared to the initial state. The melting depth of the green laser appears to be only a few micrometers, indicating that the melt pool is eventually not deep enough to completely melt the DBC metallization during the PBF-LB/M process. The melt pool created during the process is lenticular and relatively flat. For the infrared laser sample, the grain structure on the front side of the DBC substrate below the AM sample is completely changed upon PBF-LB/M processing compared to the initial state. In the respective area the microstructure of the metallization is very similar to the microstructure of the AM sample. This indicates that the melting depth of the infrared laser is so high that the entire metallization thickness is remelted and, thus, significantly higher than the melting depth of the green laser. In the area surrounding the AM sample, the grain structure of the metallization is not influenced by the PBF-LB/M process. The melt pool of the infrared laser sample cannot be visualized. Due to the small focal diameter of the infrared laser, it is assumed that the width of the melt pool is significantly smaller than the width of the melt pool with the green laser.

In addition, the local texture of the samples was analyzed for both lasers. Figure 6a demonstrate the sample manufactured with the green laser and Figure 6b the sample manufactured with the infrared laser. Overall, hardly any preferred orientation can be seen (texture intensities have not been calculated). There appears to be a change of grain appearance depending on whether the bulk volume or the top surface of the sample is considered. However, this change cannot be quantitatively evaluated based on data available. As already described in the microstructure analysis, the hatching in the PBF-LB/M process determines the microstructure of the infrared laser sample. An alignment of the grains in hatch

direction occurs, controlled by the thermal gradient during the laser movement. Such an alignment is not visible within the green laser sample. In summary, the results provide an initial impression of orientation distribution in the microstructure of the samples. Further analysis is required to enable a precise evaluation of the texture. However, these are beyond the scope of present work.

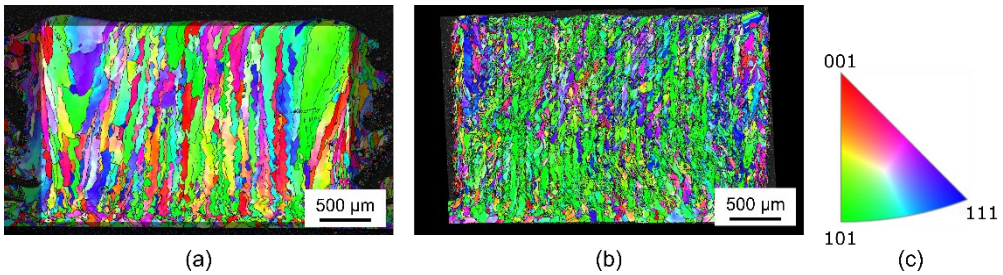

Figure 6: Microstructural orientation in cross section of samples manufactured with high-density process parameter sets for both lasers: (a) the green laser and (b) the infrared laser as well as (c) the inverse pole figure colour coding legend.

As the thermal conductivity is crucial for applications in power electronics, Figure 7 shows a direct comparison of the conductivity measurements of the AM samples of both lasers compared to the reference value of the conventionally processed bulk copper sample.

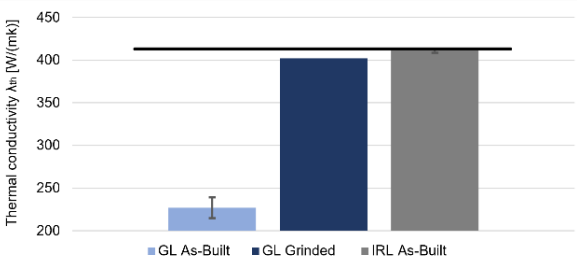

Figure 7: Thermal conductivity of different AM samples in comparison to bulk copper sample as reference: as-built and grinded samples manufactured with green laser (GL) as well as as-built samples manufactured with infrared laser (IRL).

With a thermal conductivity of 406 W/(mK), the value of the conventionally manufactured sample corresponds to the literature value. The thermal conductivity measured for the as-built AM samples manufactured with the green laser is around 227 W/(mK) and is therefore 45 % lower than the reference value. After removal of the sintered particles on the side surfaces, when only the dense core of the sample is considered, a thermal conductivity of 402 W/(mK) was measured. The as-built samples of the infrared laser are characterized by a high geometric accuracy, featuring far less sintered particles on the side surfaces. Thus, the thermal conductivity can be related to an almost well-defined cross-sectional area already in as-built condition. With around 411 W/(mK), the thermal conductivity is similar to the thermal conductivity of the (ground) green laser sample and the reference value. Due to the high sample density, thermal conductivities being equal to conventionally manufactured copper were achieved for both lasers. However, due to the dependence of the thermal conductivity to the cross-sectional area, the porous rim of the as-built green laser sample has a significant effect on the experimentally determined results, eventually leading to a strong decrease of the calculated value in as-built condition.

3.2. Summarizing discussion of results

The present study directly compares pure copper processed with a green laser and an infrared laser in the same PBF-LB/M machinery, ensuring equal boundary conditions in both cases. With the green laser it was not possible to manufacture samples without delamination on top of a DBC substrate with a laser power of less than 400 W, regardless of the scanning speed analyzed. For the infrared laser, at least a laser power of 300 W was required. Due to the low absorptivity, only a small share of the energy applied in the PBF-LB/M process is available for melting the powder (Horn et al. 2022). Due to the high thermal conductivity of copper, the applied heat is quickly dissipated from the molten pool into the surrounding powder and is not available for melting the powder (Campagnoli et al. 2021). For both lasers, a reduction in the scanning speed at low laser power cannot compensate a too low energy input in the PBF-LB/M process. As a first conclusion, the energy input is indeed dominated by the laser power applied. The process window for manufacturing samples on the DBC substrate is narrow for both laser types. With the green laser, the physically available laser power is the limiting factor. When using the infrared laser, increasing the laser power too values above 500 W leads to damage of the DBC substrate. Despite

the increased absorption, the volume energy density required for the green laser is significantly higher than the volume energy density required for the infrared laser. The established calculation of the volume energy density (see Equation (1)), mostly used in literature, does not take the focus diameter into account (Prashanth et al. 2017). Due to the large focal diameter of the green laser, the laser power applied in the PBF-LB/M process is distributed over a large area. This eventually results in a low power density within the process. In contrast, the infrared laser is characterized by a small focal diameter, which enables a focused application of the energy and therefore a higher power density within the process. When using the green laser, sintered particles occur on the side surfaces of all samples, regardless of the process combination considered. This leads to a low dimensional accuracy and a high surface roughness of the manufactured structures. In contrast, the samples manufactured with the infrared laser are characterized by a high geometric accuracy, and hardly any sintered particles are observed on the side surfaces of the samples. The green laser exhibits a flattened Gaussian intensity distribution and a large focal diameter due to its relatively poor beam quality. The intensity in the edge area of the green laser is so high that the powder particles in the surrounding area of the samples are heated and sintered to the side surfaces of the samples. Moreover, due to the high thermal conductivity of copper, the powder in the surrounding area of the manufactured sample is additionally heated by the dissipated heat during the PBF-LB/M process, which supports the sintering of the powder particles. With the infrared laser, however, the energy input is highly focused and the power intensity in the outer area of the laser is almost Zero. The energy input in the center of the laser beam is so high that the copper powder is completely melted. In the outer area of the laser beam, the energy input is not sufficient to sinter a high number of powder particles to the side surfaces of the samples. These effects result in a sharply defined contour and a high dimensional accuracy.

The microstructure analysis of the green laser sample reveals a lenticular and flat melt pool geometry as well as a low melting depth, eventually indicating that the copper processing occurs in the thermal conduction mode (Wang und Zou 2019). In thermal conduction mode, the energy in the PBF-LB/M process is primarily absorbed at the powder layer surface (Wang und Zou 2019). Due to the heat conduction and the high thermal conductivity of copper, the energy is distributed within the powder layer, forming a melt pool (Wang und Zou 2019). Due to the small focus diameter of the infrared laser, it is assumed that the melt pool is considerably smaller than the melt pool of the green laser. As the whole metallization of the DBC substrate is remelted during the PBF-LB/M process, the melting depth of the infrared laser is significantly higher than the melting depth of the green laser. For laser welding, this narrow but deep melt pool geometry indicates a processing of copper in the deep welding mode. In case of traditional laser welding, the transition from heat conduction welding to deep penetration welding can be realized by increasing the power density of the laser radiation (Wang und Zou 2019). When a certain threshold is reached, the vaporization temperature of the material is exceeded. The formation of vapor channels, a so-called keyhole, can occur inside the material (Wang und Zou 2019). This causes the laser radiation to be directed deeper into the material and increases the absorption. Using the infrared laser instead of the green laser within the PBF-LB/M process changes the power density and the intensity distribution of the laser significantly. Eventually, this leads to the transition between the different melting modes.

The top surface of the green laser sample exhibits significant surface roughness and a high number of melting defects. In addition, the analysis of the microstructure reveals a low melting depth associated with the green laser, as detailed before. The poor surface quality observed on the top of the samples is potentially a result of the Plateau-Rayleigh instability. Due to the limited melting depth, during PBF-LB/M processing droplets generate on top of the DBC metallization (and in case of a higher build height the underlying layers), which partially wet the surface. Due to Plateau-Rayleigh instability, the surface energy is reduced by splitting an elongated cylindrical melt pool into multiple droplet-like formations (Heeling 2018). Consequently, the melting behavior, particularly within the lower layers, becomes highly unstable. This instability propagates upwards, resulting in an accumulation of surface roughness with increasing build height. With the infrared laser, a significantly higher melting depth is realized, evident from microstructure analysis of the samples. When the melt pool is generated, the underlying DBC metallization (or previously processed layers) are completely melted and wetted. This leads to a high surface quality from layer to layer within the sample and, thus, to a high surface quality on the top surface of the samples. The grain growth in the direction of the samples is caused by the layerwise manufacturing and the resulting thermal gradient within the sample. Thermomechanically, the highest heat transfer occurs within a solid material. In the PBF-LB/M process, the solidified layers are located below the current melt pool, which enables the heat transfer in the sample alongside the build direction. The high thermal conductivity of the copper metallization also leads to a rapid dissipation of heat from the AM structure into the DBC substrate and, thus, further increases the thermal gradient. Neither the green laser sample nor the infrared laser sample are characterized by pronounced texture. From data obtained it can be derived that the solidification alongside the laser movement direction within a layer is more dominant than the effect of the thermal gradient in the build direction of the samples. However, at this point further in-depth analysis is to be done in future.

For both the green and the infrared laser, no cracks occur in the ceramic of the DBC substrate in the single sample layout. Within this layout, the thermal input into the DBC substrate and the residual stress states introduced during the PBF-LB/M process are therefore below a threshold. A detailed examination of the impact of the PBF-LB/M process on the DBC substrate

across various layouts, including the crack formation in the DBC ceramic, has significant scientific and industrial relevance. As already detailed in the introduction, these cracks, regardless of their type or size, compromise the electrical insulation capabilities of the ceramic layer and must be prevented. Additionally, in-depth studies on the thermal properties—such as conductivity and coefficient of expansion—of the different substrate materials would be valuable. However, these aspects are beyond the scope of the present investigation and, thus, will be addressed in future publications.

The key findings and microstructure formation mechanisms are summarized in the schematic presented in Figure 8. Here, Figure 8a illustrates the PBF-LB/M process with the green laser, while Figure 8b depicts the PBF-LB/M process with the infrared laser. Process parameters that lead to the maximum sample densities are the basis for the illustrations. A detailed explanation of all physical interactions would necessitate additional numerical studies for both wavelengths. Thermomechanical simulations examining the interactions between the PBF-LB/M process and the ceramic-based DBC substrate, along with the resulting thermal gradients, would be valuable. However, these aspects are beyond the scope of this publication and will be explored in future works.

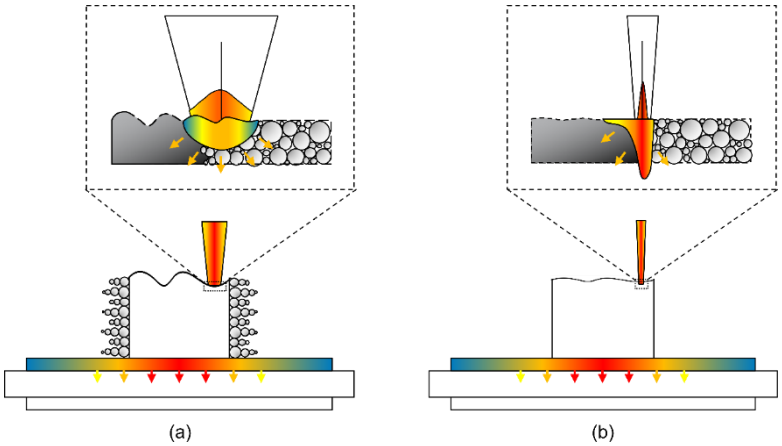

Figure 8: Schematic illustration of the key results and their formation mechanisms within the PBF-LB/M process on ceramic-based DBC substrates: (a) green laser and (b) infrared laser.

4. Conclusions

Power electronics include small functional metallic structures, preferably made of pure copper, which are built on delicate ceramic-based DBC substrates with both sided copper metallization. The present publication introduces a novel AM approach, employing the PBF-LB/M process to directly manufacture the functional structures on the DBC substrate, thereby reducing manufacturing costs and effort. The work presented compares the processing of pure copper powder using two different lasers, one with a green wavelength and one with an infrared wavelength. Both lasers were implemented in the same PBF-LB/M machinery, allowing a direct comparison of both wavelengths under similar boundary conditions. By varying laser power and scanning speed, a broad range of volume energy densities were systematically examined in the process development that aimed to achieve maximum sample density. Individual samples produced with high-density process parameters for both lasers, i.e., those obtained after process optimization, were evaluated to determine the impact of the laser wavelength on the sample properties, focusing on optical appearance, microstructure and thermal conductivity. The study presented focused on the properties of the AM structures and their interface with the DBC substrate. Unlike previous literature, the functional structures discussed here are only a few millimeters in size, and specifically adapted to the needs of power electronics applications.

The key results can be summarized as follows:

- Successful manufacturing of samples with densities higher than 99.9 % and complete bonding to the DBC substrate with both lasers is achieved.
- High geometric accuracy of samples processed with the infrared laser, due to its high laser power density and its sharp gaussian intensity distribution, is seen.
- A significantly reduced geometric accuracy of the green laser processed samples, due to its high beam intensity in the outer area of the laser beam in combination with the high thermal conductivity of copper, is found.
- The microstructure of the infrared laser samples is dominated by hatching and laser movement. Here a significant effect of the laser intensity profile and laser power density on the temperature profile within the sample prevails.
- The structures manufactured are characterized by high thermal conductivity due to the high sample densities achieved with both lasers.

Acknowledgements

This work was supported by the Horizon Europe research and innovation program under Grant 101138289, 'Enabling Laser Powder Bed Fusion for Large Scale Production of Multi-Material Components', acronym GlobalAM.

References

Campagnoli, Marta Roccetti; Galati, Manuela; Saboori, Abdollah (2021): On the processability of copper components via powder-based additive manufacturing processes: Potentials, challenges and feasible solutions. In: *Journal of Manufacturing Processes* 72. DOI: 10.1016/j.jmapro.2021.10.038.

Colopi, Matteo; Demir, Ali Gökhan; Caprio, Leonardo; Previtali, Barbara (2019): Limits and solutions in processing pure Cu via selective laser melting using a high-power single-mode fiber laser. In: *The International Journal of Advanced Manufacturing Technology* 104. DOI: 10.1007/s00170-019-04015-3.

Domine, Aymeric; Verdy, Christophe; Penaud, Corentin; Vitu, Ludovic; Fenineche, Nouredine; Dembinski, Lucas (2023): Selective laser melting (SLM) of pure copper using 515-nm green laser: from single track analysis to mechanical and electrical characterization. In: *Int J Adv Manuf Technol*. DOI: 10.1007/s00170-023-12338-5.

Gaiser, Patrick; Klingler, Markus; Wilde, Jürgen (2020): The influence of strain hardening of copper on the crack path in Cu/Al2O3/Cu direct bonded copper substrates. In: *International Journal of Fatigue* 140. DOI: 10.1016/j.ijfatigue.2020.105821.

Ghasemi-Tabasi, Hossein; Jhabvala, Jamasp; Boillat, Eric; Ivas, Toni; Drissi-Daoudi, Rita; Logé, Roland E. (2020): An effective rule for translating optimal selective laser melting processing parameters from one material to another. In: *Additive Manufacturing* 36, S. 101496. DOI: 10.1016/j.addma.2020.101496.

Gruber, Samira; Stepien, Lukas; López, Elena; Brueckner, Frank; Leyens, Christoph (2021): Physical and Geometrical Properties of Additively Manufactured Pure Copper Samples Using a Green Laser Source. In: *Materials* 14 (13). DOI: 10.3390/ma14133642.

Hecht, Christoph; Ockel, Manuela; Stoll, Thomas; Franke, Jörg (2024): Fabrication of metal-ceramic substrates by laser powder bed fusion using a high-power green laser and high temperature preheating. In: Laser 3D Manufacturing: Spie Lase. Online verfügbar unter https://www.spiedigitallibrary.org/conference-proceedings-of-spie/12876/3001350/Fabrication-of-metal-ceramic-substrates-by-laser-powder-bed-fusion/10.1117/12.3001350.full.

Heeling, Thorsten (2018): Synchronized Two-Beam Strategies for Selective Laser Melting. Doctoral Thesis. In: *ETH Zürich*. DOI: 10.3929/ethz-b-000270330.

Horn, Max; Schmitt, Matthias; Schafnitzel, Mario; van Husen, Anne; Wagenblast, Philipp; Auernhammer, Stefan et al. (2022): Powder Bed Fusion of highly filigree copper features using a green laser. In: *Procedia Engineering* 111. DOI: 10.1016/j.procir.2022.08.135.

Hromadka, Karel; Stulik, Jiri; Reboun, Jan; Hamacek, Ales (2014): DBC Technology for Low Cost Power Electronic Substrate Manufacturing. In: *Procedia Engineering* 69. DOI: 10.1016/j.proeng.2014.03.107.

Ikeshoji, Toshi-Taka; Nakamura, Kazuya; Yonehara, Makiko; Imai, Ken; Kyogoku, Hideki (2018): Selective Laser Melting of Pure Copper. In: *JOM* 70 (3), S. 396–400. DOI: 10.1007/s11837-017-2695-x.

Jadhav, S. D.; Dadbakhsh, S.; Goossens, L.; Kruth, J-P; van Humbeeck, J.; Vanmeensel, K. (2019): Influence of selective laser melting process parameters on texture evolution in pure copper. In: *Journal of Materials Processing Technology* 270 (111). DOI: 10.1016/j.jmatprotec.2019.02.022.

Lin, Yusheng; Liu, Yong (2020): Automotive High Power Module with Spacer on Die Bottom (Flip Chip) or Die Top (Wire Bond). In: PCIM Europe digital days; International Exhibition and Conference for Power Electronics, Intelligent Motion, Renewable Energy and Energy Management.

Lykov, P. A.; Safonov, E. V.; Akhmedianov, A. M. (2016): Selective Laser Melting of Copper. In: *Materials Science Forum* 843. DOI: 10.4028/www.scientific.net/MSF.843.284.

Megahed, Sandra; Koch, Raphael; Schleifenbaum, Johannes Henrich (2022): Laser Powder Bed Fusion Tool Repair: Statistical

Analysis of 1.2343/H11 Tool Steel Process Parameters and Microstructural Analysis of the Repair Interface. In: *Journal of Manufacturing and Materials Processing* 6. DOI: 10.3390/jmmp6060139.

Nordet, Guillaume; Gorny, Cyril; Coste, Frédéric; Lapouge, Pierre; Effernelli, Albin; Blanchet, Etienne; Peyre, Patrice (2024): Influence of laser wavelength on the powder bed fusion of pure copper. In: *Progress in Additive Manufacturing*. DOI: 10.1007/s40964-024-00720-y.

Prashanth, K. G.; Scudino, S.; Maity, T.; Das, J.; Eckert, J. (2017): Is the energy density a reliable parameter for materials synthesis by selective laser melting? In: *Materials Research Letters* 5 (6). DOI: 10.1080/21663831.2017.1299808.

Punzel, Eric; Hugger, Florian; Dörringer, Robert; Dinkelbach, Thorm Lembit; Bürger, Andreas (2020): Comparison of different system technologies for continuous-wave laser beam welding of copper. In: *Procedia CIRP* 94. DOI: 10.1016/j.procir.2020.09.081.

Rogers Corporation (2025): curamik Ceramic Substrates. Product Information & Data Sheet. Online verfügbar unter https://www.rogerscorp.com/advanced-electronics-solutions/curamik-ceramic-substrates/curamik-power, zuletzt geprüft am 24.04.2025.

Shi, Bufan; Ramones, Anna Isabel; Liu, Yingxu; Wang, Haoran; Li, Yu; Pischinger, Stefan; Andert, Jakob (2023): A review of silicon carbide MOSFETs in electrified vehicles: Application, challenges, and future development. In: *IET Power Electronics* 16 (12). DOI: 10.1049/pel2.12524.

Stoll, Thomas; Kirstein, Matthias; Franke, Jörg (2019): A novel approach of copper-ceramic-joints manufactured by selective laser melting. In:. Material Technologies and Applications to Optics, Structures, Components, and Sub-Systems, Bd. 1110101: SPIE Opical Engineering + Applications. Online verfügbar unter https://www.spiedigitallibrary.org/conference-proceedings-of-spie/11101/2529422/A-novel-approach-of-copper-ceramic-joints-manufactured-by-selective/10.1117/12.2529422.full.

Wang, D.; Liu, Zhenyu; Deng, Guowei; Zhou, Xin; Li, Sheng; Wang, Haoliang et al. (2024): A laser powder bed fusion–based methodology for repairing damaged nickel-based turbine blades: Investigation of interfacial characteristics and hot isostatic pressing treatment. In: *Materials Characterization* 212. DOI: 10.1016/j.matchar.2024.113948.

Wang, Hongze; Zou, Yu (2019): Microscale interaction between laser and metal powder in powder-bed additive manufacturing: Conduction mode versus keyhole mode. In: *International Journal of Heat and Mass Transfer* 142. DOI: 10.1016/j.ijheatmasstransfer.2019.118473.

Appendix A

Appendix A1: Overview image and dimensions of the as-delivered DBC substrate: (a) front side, (b) back side and (c) cross section.

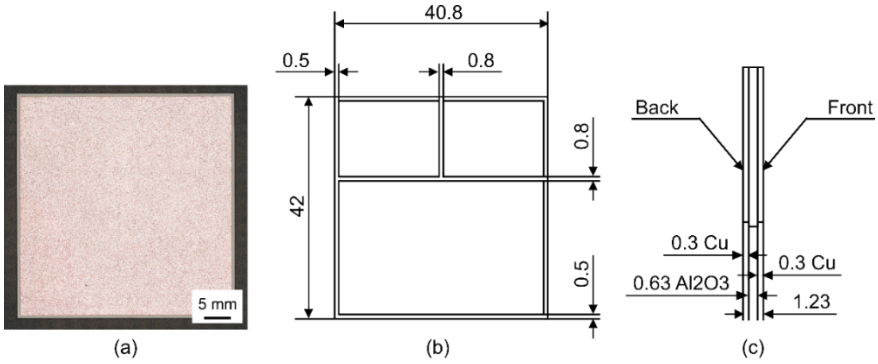

Appendix A2: Comparison of the two lasers in the machine configuration, used in the present investigations.

Specification			Green laser	Infrared laser
Type			TruDisk 1020 disc laser	YLR-1000-WC fiber laser
Manufacturer			Trumpf SE + Co KG, Ditzingen, Germany	IPG Photonics Corporation, Marlborough, Massachusetts, United States
Operation mode			Multi-mode	Single-mode
Wavelength	λ	nm	515	1070
Beam quality	M^2	-	12.8	1.1
Laser beam diameter	d_f	µm	330	60
Max. laser power	P	W	800	800
Max. power density	P/A_f	W/mm²	9353	282942

Appendix A3: Varied and constant PBF-LB/M process parameters for both lasers as part of the parameter study.

Process parameter			Green laser		Infrared laser	
			Value	Increment	Value	Increment
Laser power	P	W	200 – 800	200	200 – 600	100
Scanning speed	v	mm/s	200 – 800	200	600 – 900	100
Volume energy	Ev	J/mm³	83.3 – 1333.3		92.6 – 416.7	
Hatch distance	h	mm	0.10		0.08	
Layer thickness	s	mm	0.03		0.03	
Rotation angle	-	°	90		90	